ACS OMEGA

http://pubs.acs.org/journal/acsodf

Article

Composite PVK/SLGO As Matrix for MALDI-TOF MS Detection of Small Molecules in Dual-Ion Mode

Xiuying Chen, Yonghui Wang, Yuanyuan Luo, Zhixian Gao, Tie Han,* and Huanying Zhou*

Cite This: *ACS Omega* 2022, 7, 39028−39038

Read Online

ACCESS | Metrics & More | Article Recommendations | Supporting Information

ABSTRACT: Currently, most matrices developed for matrix-assisted laser desorption/ionization mass spectrometry (MALDI-TOF MS) for small-molecule detection are only suitable for the positive or negative ion mode and not the dual-ion mode, except for carbon-based nanomaterials. The lone-pair electrons on the N atom in poly n-vinylcarbazole (PVK) can serve as a Lewis base with strong electron-donation effects, which is favorable for negative ion mode detection. The surface of single-layer graphene oxide (SLGO) contains many oxygen atoms in carboxyl and hydroxyl groups that act as Lewis acids and thereby provides favorable protonation sites for positive ion mode detection. In this study, composite PVK/SLGO was prepared by combining the advantages of amorphous PVK and SLGO. PVK/SLGO was tested as a novel matrix for positive- and negative-ion-mode MALDI-TOF MS for the analysis of amino acids, nucleic acid bases, environmental endocrine disruptors, antibiotics, and various small molecules. PVK/SLGO was compared with PVK, SLGO, and commercially available matrices of 9-aminoacridine (9-AA) and α-cyano-4-hydroxycinnamic acid (CHCA). The PVK/SLGO matrix was demonstrated to be suitable for the positive and negative ion modes, exhibiting high signal intensity and detection sensitivity without background interference. The limits of detection of the aforementioned molecules ranged from 0.1 to 0.0001 and 0.01 to 0.0001 mg/mL in the positive and negative ion modes, respectively. The quantitative determination of enrofloxacin in milk was realized using an internal standard method with a linear range of 0.0001−0.1 mg/mL (R^2 = 0.9991). Furthermore, the PVK/SLGO matrix exhibited high salt tolerance (up to 1000 mmol/L) and stability over 28 consecutive days. Studies regarding its ionization mechanism revealed that the good performance originates from the combined materials acting synergistically. This study provides a foundation for developing bimodal composite matrices and further expands the scope of PVK/SLGO applications.

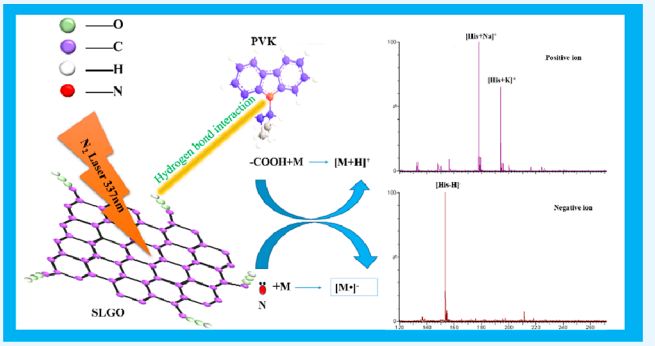

1. INTRODUCTION

Matrix-assisted laser desorption/ionization mass spectrometry (MALDI-TOF MS) is a soft ionization technique[1] that is effective for the detection and identification of biological samples because of the low sample volume required, rapid analysis, and high throughput. However, few challenges still impede the realization of positive- and negative-dual-ion-mode MALDI-TOF MS for the analysis of small molecules using composite materials as a matrix. Except for carbon-based nanomaterials, which are suitable for the positive and negative dual-ion mode detection of small molecules, most MALDI matrices are amenable to only single-mode detection.

Recently, the development of MALDI matrices based on novel nanomaterials has rapidly increased in popularity. Many inorganic nanoparticles have been explored as MALDI matrices, including metal−organic frameworks,[2] hybrid materials,[3] covalent organic frameworks,[4] porous silicon,[5] metal and metal oxide nanoparticles,[6−9] and carbon-based nanomaterials with different compositions and morphologies.[10−12] In particular, carbon-based nanomaterials, including graphite, graphene, fullerene, carbon nanotubes, and diamond nanowires, have attracted significant interest for applications in laser desorption/ionization owing to their excellent charge mobility and unique optical absorption characteristics.[12−15] Graphene exhibits several advantages as a MALDI matrix, including its simple single-layer structure and unique conductivity[16,17] that can enhance laser desorption/ionization efficiency. In addition, graphene has a large specific surface area[18] and many active sites,[19,20] which facilitate efficient absorption and effectively eliminate the interference introduced by traditional organic matrices. Graphene oxide, obtained from the oxidation of graphene, has a special chemical structure consisting of carbon atoms, oxygen-containing functional groups, cavities, and defects. Its unique

Received: July 28, 2022
Accepted: October 3, 2022
Published: October 21, 2022

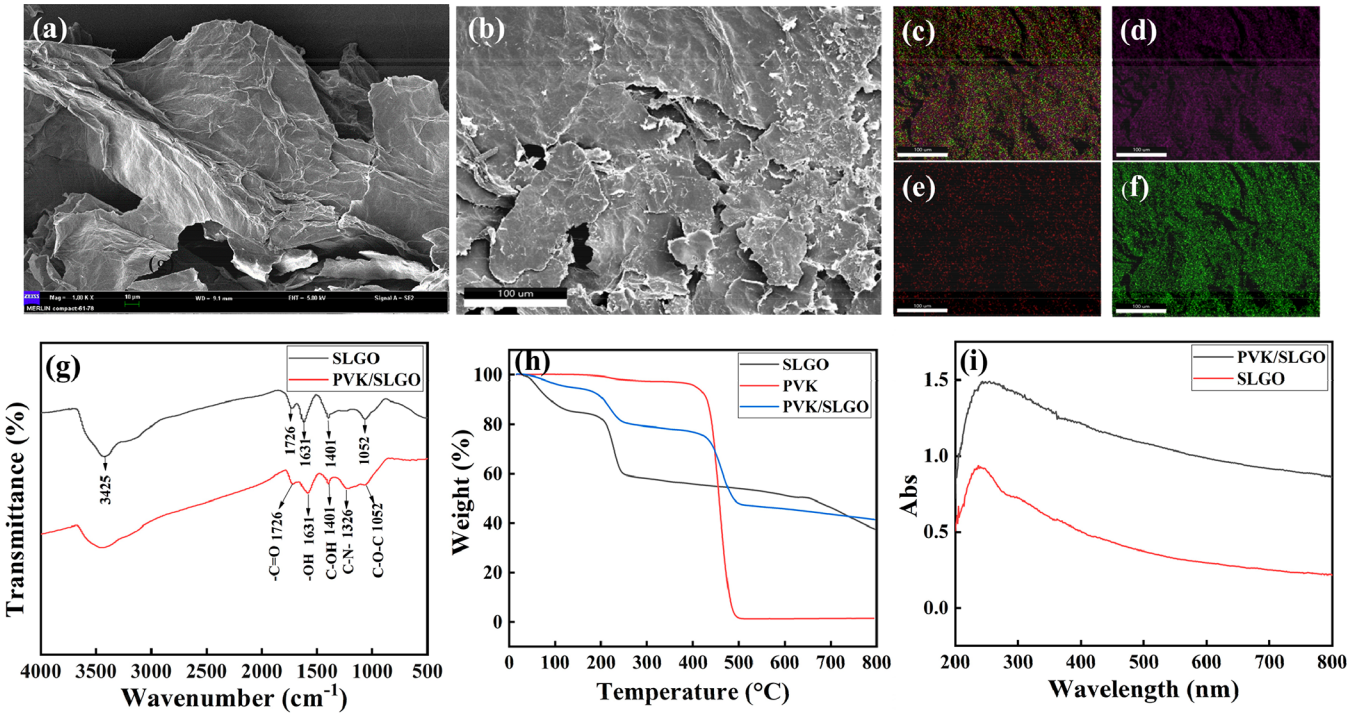

Figure 1. SEM image of (a) SLGO and (b) PVK/SLGO. (c) SEM elemental mapping diagrams of PVK/SLGO. (d–f) SEM elemental mapping diagrams of C, O, and N in PVK/SLGO. (g) FT-IR spectra of SLGO and PVK/SLGO. (h) TGA curves of SLGO, PVK, and PVK/SLGO and (i) UV–vis spectra of SLGO and PVK/SLGO.

planar structure and extremely large specific surface area result in a special energy state distribution in its electronic structure. These features are beneficial for applications in optical fields owing to the energy gap between the conduction and valence bands.[21−25]

Graphene oxide exhibits significant absorption over the entire spectral region from UV to IR owing to its numerous oxygen-containing functional groups.[26] SLGO is a single sheet of graphene oxide separated via mechanical decidualization.[27−29] Its composition and structure are similar to those of graphene oxide,[30,31] including its large specific surface area, easy desorption/ionization, and strong UV absorption. It can function simultaneously as a matrix and an adsorbent that can effectively eliminate matrix-related interference peaks in the low-quality region. In addition, the oxygen atoms of the numerous carboxyl and hydroxyl groups on SLGO can serve as Lewis acids, providing protonation sites essential for the MALDI matrices designed for small-molecule analysis in the positive ion mode. The N atom in the amorphous PVK carbazole ring contains sp^2 lone pairs, which can serve as Lewis bases and accept protons from the analytes. Amorphous PVK as a matrix exhibits high desorption/ionization efficiency in the negative ion mode. As a MALDI-TOF MS matrix, it has proven effective in qualitative and quantitative small-molecule analysis with wide applicability. However, PVK is only suitable for the negative ion mode, and the matrix self-interference peak is observed at m/z 165.[32]

Compared to single-mode matrices, dual-mode matrices have wider applicability with a high number of detectable small molecules. Few substrates can be used for small-molecule detection in the positive and negative dual-ion mode. Wang et al.[33] prepared porous amorphous carbon-coated, phosphorus, nitrogen codoped graphene with P–O surface groups using aerogels formed with phytic acid, polyaniline, and electrochemically exfoliated graphene as raw materials. Its subsequent application as a MALDI matrix allowed for the positive and negative dual-ion mode detection of small molecules, including amino acids, small peptides, sugars, drugs, and environmental pollutants, with high sensitivity. Nie et al.[34] synthesized various carbon quantum dots (CDs) by sodium borohydride reduction, microwave synthesis, and thermal oxidation. CD-based matrices prepared by sodium borohydride reduction can simultaneously detect amino acids, oligopeptides, neutral oligosaccharides, β-agonists, fatty acids, and polymers in both positive and negative ion modes. MALDI MS analysis using isotopic internal standard methods has also been demonstrated for the quantitative determination of glucose in serum and uric acid in urine. Hayes et al.[35] used 3-hydroxypicolinic acid (HPA) as a MALDI matrix and successfully distinguished between sophorolipid forms by detection in both positive and negative ion modes. Lissel et al.[36] synthesized two amorphous copolymers as MALDI matrices to detect various small molecules, including reserpine, tetraethylammonium chloride, coumaphos, cholic acid, citric acid, and phenylalanine, in the positive and negative dual-ion mode. Lissel et al.[37] synthesized four conjugated polymers as bimodal matrices for multiple small-molecule analyses. In addition, coronal and sagittal slices of rat brain were imaged and visualized using a P3DDT substrate in the negative electrode reflection mode. Therefore, it is important to develop novel matrices that limit background interference and can be used for the positive and negative dual-ion mode determination of small molecules by MALDI-TOF MS.

Composite matrices improve desorption and ionization processes,[38] facilitate uniform sample matrix cocrystallization,[39] expand detection ranges,[40] and improve detection sensitivity[41] by suppressing matrix clustering and fragmentation. Chen et al.[42] developed a novel binary matrix composed

https://doi.org/10.1021/acsomega.2c04772
ACS Omega 2022, 7, 39028−39038

of 9-AA and CDs for small-molecule determination by MALDI-TOF MS. The matrix and sample underwent uniform cocrystallization, improving point-to-point reproducibility and detection sensitivity. Moreover, the CDs acted as a matrix additive to suppress 9-AA ionization.

In this study, a novel composite matrix (PVK/SLGO) composed of SLGO and PVK was developed for the MALDI-TOF MS analysis of small molecules by combining the excellent characteristics of SLGO and advantages of the composite matrix. To evaluate its matrix performance, various small molecules, including amino acids, nucleic acid bases, quinolone antibiotics, and environmental endocrine disruptors, were examined and compared with traditional matrices like 9-A and CHCA and precursor materials SLGO and PVK. The composite-PVK/SLGO-assisted MALDI-TOF MS method was applied for small-molecule detection in the dual-ion mode without background interference, and it exhibited many advantages, including simplicity, rapidity, high sensitivity, reproducibility, and a wide detection range. The salt tolerance and stability of the novel matrix were further evaluated, and the results demonstrated its superiority. Finally, the ionization mechanism of the composite PVK/SLGO matrix was discussed in detail. Novel substrates for MALDI-TOF MS were successfully developed in this study while defining the application range of the newly developed composite, PVK/SLGO.

2. RESULTS AND DISCUSSION

2.1. Characterization of PVK/SLGO. The morphologies and structures of SLGO and the PVK/SLGO composite were examined by scanning electron microscopy (SEM) and Energy Dispersive X-ray Spectroscopy (EDX) analyses. As shown in Figure 1a, the surface of SLGO exhibited a single-layered wrinkled morphology, while the wrinkled boundaries were observed to be step-like and laminated. Figure 1b shows that the PVK/SLGO composites maintained this single-layered flake structure with increased surface roughness. The white amorphous PVK attached to the surface of the SLGO flake, indicating successful synthesis of the PVK/SLGO composites. EDX elemental analysis (Figure 1c) demonstrated a uniform dispersion of carbon, oxygen, and nitrogen, which corresponded to the elemental composition of composite materials in PVK/SLGO (Figure 1d−f). The X-ray diffraction (XRD) patterns of SLGO and PVK/SLGO are shown in Figure S1, where the strong diffraction peak at 2θ = 10.6° in SLGO corresponds to the (001) plane peak of graphene oxide.[43] From the literature,[44] this characteristic XRD peak arises from SLGO; a small graphite (002) characteristic peak was also observed at 42.44°,[44] indicating that most of the graphene exists as SLGO. The 2θ diffraction peak corresponding to PVK/SLGO appeared at ∼12.96°, exhibiting a shift to the right relative to the SLGO (001) crystal plane peak and a significantly weaker intensity. Simultaneously, in the PVK/SLGO medium, broad 2θ diffraction peaks between 15° and 25° arising from PVK weakened. The elemental compositions of SLGO and PVK/SLGO were further examined by X-ray photoelectron spectroscopy (XPS; Figure S2). Clearly, PVK/SLGO exhibits C, O, and N peaks, while SLGO only exhibits peaks originating from C and O. FT-IR images of SLGO and PVK/SLGO are presented in Figure 1g, showing a strong and wide absorption peak at ∼3401 cm^{-1} corresponding to the −OH stretching vibration of water adsorbed between SLGO layers. The peak at approximately ∼1726 cm^{-1} was attributed to −C═O vibrations on the SLGO surface, indicating that −COOH and −C═O were present in SLGO.[45] The peak at 1631 cm^{-1} corresponds to the O−H bending vibration and the backbone vibrations of the epoxy group and six-membered ring.[46] The peak at 1401 cm^{-1} was assigned to the C−OH stretching vibration on the SLGO surface, indicating that the SLGO surface contained hydroxyl groups. The peak at 1052 cm^{-1} originates from the aromatic C−O−C stretching vibration. In addition to the SLGO-related peaks, PVK/SLGO exhibited an absorption peak at 1326 cm^{-1} corresponding to the C−N stretching vibration in the carbazole ring. These findings indicate that SLGO and PVK were successfully blended to form PVK/SLGO composites. The Raman spectra in Figure S3 show a 2D band peak at 2703 cm^{-1} and a G + D band peak at 2948 cm^{-1}. The 2D and D + G peaks indicate that the prepared graphene oxide adopted a monolayer structure.[47] The I_D/I_G ratio of PVK/SLGO was higher than that of SLGO, while the D peak at 1358 cm^{-1} slightly shifted and exhibited a higher intensity. Thermogravimetric analyses (TGA) of SLGO, PVK, and PVK/SLGO were performed under a N_2 atmosphere (Figure 1h). At 200 °C, a 10% weight loss was observed due to solvent or surface water molecule evaporation from the SLGO surface or interlayer. The weight loss of ∼10% at 230 °C likely originated from the decomposition reaction of unstable oxygen-containing functional groups in SLGO to generate CO_2, CO, and H_2O. At 458 °C, a 30% weight loss was observed due to the thermal decomposition of some unstable groups in PVK. These results indicate that the PVK/SLGO composite was successfully synthesized. As shown in Figure 1i, the strong absorption peak of PVK/SLGO was red-shifted compared that of SLGO, indicating that PVK was successfully attached to the functionalized SLGO surface and altered the material structure. The red shift is likely due to the modification of poly(*N*-vinyl carbazole) on the SLGO. The carbazole contains $\pi-\pi$ conjugation, and the surface of the SLGO contains many carboxyl groups. The nitrogen atom in the poly(*N*-vinyl carbazole) contains lone-pair electrons, allowing hydrogen bonds to form between the nitrogen and hydrogen atoms in the carboxyl group and resulting in the red shift. Furthermore, PVK/SLGO exhibited strong absorption in the near-UV region (∼250 nm), indicating its potential for absorbing energy from a laser source at 337 nm and transferring it to an analyte. The diffuse reflectance spectroscopy results of PVK/SLGO and SLGO are provided in the Supporting Information (Figure S4).

2.2. Optimisation of Experimental Conditions. The main drawback of employing traditional matrices for detecting small molecules using MALDI-TOF MS is the emergence of significant matrix-related interference peaks in the low-molecular-weight region. In this study, different parts of the preparation process of composite material PVK@SLGO (s1, s2, s3) was monitored by LDI-MS. The preparation process of PVK@SLGO was optimized as shown in Figures S5 and S6, where s3 presented no background interference in the m/z 0−1000 range, which is important for MALDI-TOF MS matrices used for small-molecule analysis. To further confirm the performance of matrix s3, s1−s3 were tested in the positive and negative ion modes with adenine (A, m/z 135.14) and histidine (His, m/z 155.16) as representative analytes. The obtained mass spectra are shown in Figures S7 and S8. For the s3 MALDI matrix, all adenine and histidine signals were detected, and a high signal intensity and signal-to-noise ratios

https://doi.org/10.1021/acsomega.2c04772
ACS Omega 2022, 7, 39028−39038

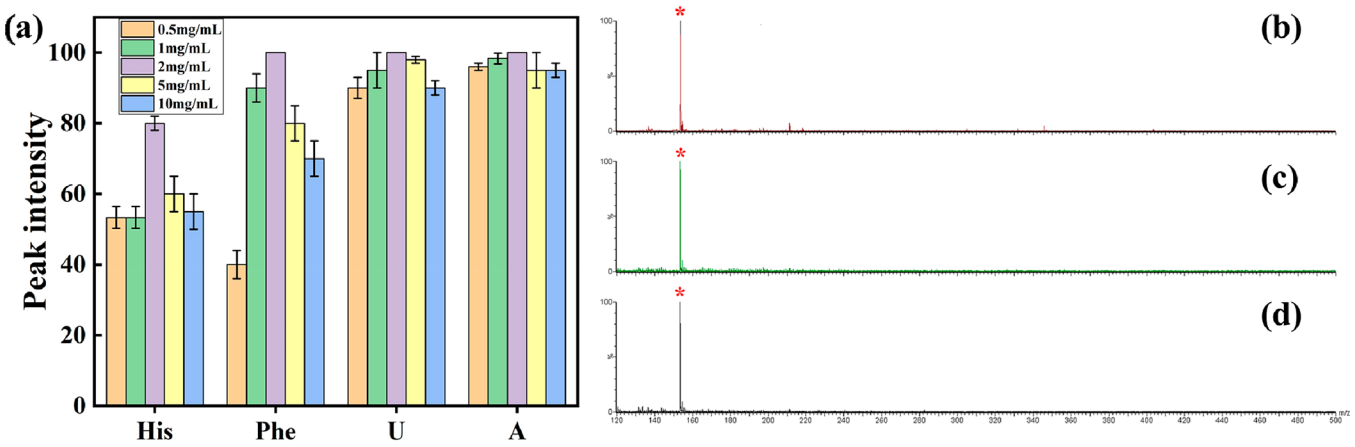

Figure 2. (a) Signal intensity of histidine, phenylalanine, uracil, and adenine at different matrix concentrations. MALDI-TOF MS profile of His with different spotting methods: (b) dried droplet method, (c) matrix priority method, and (d) sample priority method in the negative ion mode.

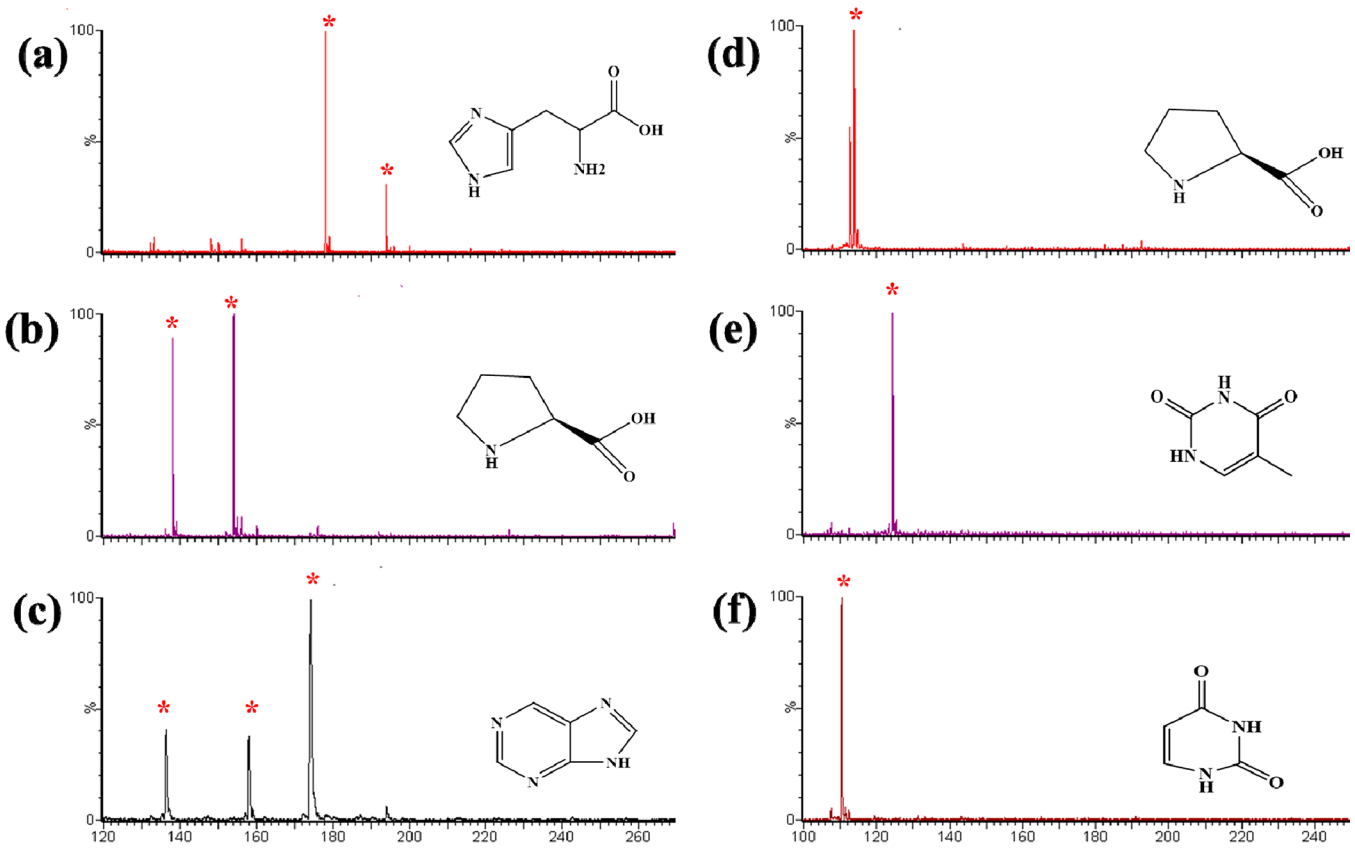

Figure 3. Mass spectra using the PVK/SLGO matrix of (a) His, (b) Pro, and (c) A in the positive ion mode and (d) Pro, (e) T, and (f) U in the negative ion mode (analyte concentration: 1 mg/mL).

were obtained. Therefore, s3 was selected as the ideal matrix for small-molecule analysis. The matrix concentration can directly affect the crystal formation uniformity between the matrix and sample and the sample dispersity, thus affecting the sensitivity and signal intensity. Therefore, it is important to select an appropriate matrix concentration. To confirm whether the matrix-assisted function was affected by different matrix concentrations, equal volumes (1 mg/mL) of His, Phe, U, and A were mixed with 0.5, 1.0, 2.0, 5.0, and 10.0 mg/mL of the PVK/SLGO matrix. The matrix concentration was optimized by comparing the absolute signal intensity of the analyte of interest. The 2 mg/mL PVK/SLGO matrix concentration exhibited the best results, and all subsequent experiments were performed at this concentration (Figure 2a). During MALDI-TOF MS analysis, the matrix/sample crystalline homogeneity significantly affects repeatability. The spotting method is often used to control matrix uniformity and sample crystallization. In this study, three spotting methods, namely, the sample priority, matrix priority, and dried droplet methods, were applied. The signal intensities obtained using these spotting methods were similar; the dried droplet spotting method exhibited operational simplicity and was hence selected for subsequent experiments (Figures 2b–d and S9). The spotting mode of the sandwich method was in

https://doi.org/10.1021/acsomega.2c04772
ACS Omega 2022, 7, 39028−39038

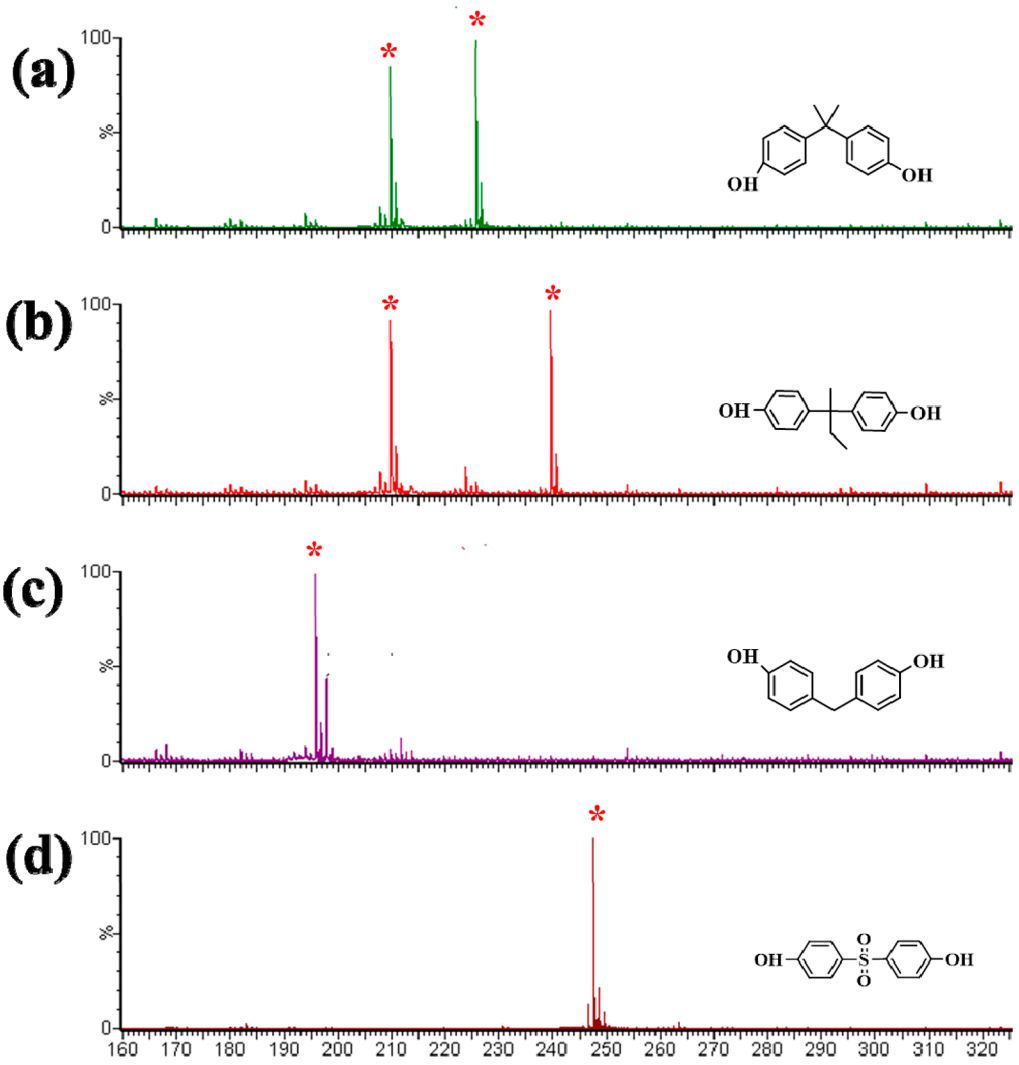

Figure 4. Negative-ion-mode MALDI MS of (A) BPA, (B) BPB, (C) BPF, and (D) BPS detected using PVK/SLGO as a matrix.

accordance with the matrix−sample−matrix order. Because the spotting mode of the matrix- and sample-priority methods was not obvious, it was further speculated that the sandwich method did not induce significant changes; hence, no further sandwich method spotting was performed.

2.3. MALDI-TOF MS of Amino Acids and Nucleic Acid Bases. CHCA is a commonly used matrix for MALDI MS. It offers excellent detection in the positive ion mode,[6] while 9-AA is an effective matrix for small-molecule detection in the negative ion mode.[48] To explore the potential of PVK/SLGO as a MALDI matrix, comparative LDI mass spectroscopy analyses were performed using CHCA, SLGO, PVK, and PVK/SLGO in the positive ion mode (Figure S10). Furthermore, LDI mass spectroscopy analyses in the negative ion mode were performed using 9-AA, SLGO, PVK, and PVK/SLGO matrices (Figure S11). The results obtained from the different matrices in both positive and negative ion modes were compared, and no matrix-associated peaks were observed in the m/z 0−1000 range when PVK/SLGO was directly ionized. Thus, adequate MALDI matrix performance for the determination of small molecules with low background interference was confirmed. To further validate the performance of PVK/SLGO as a dual-ion mode matrix, phenylalanine (MW 165.19 g/mol) was analyzed using CHCA, 9-AA, SLGO, PVK, and PVK/SLGO matrices in the positive and negative ion modes (Figure S12). When CHCA was used as a matrix in the positive ion mode, the $[M + H]^+$ ion (m/z 166.19) of phenylalanine was observed with matrix-related peaks at m/z 172 and 190 (Figure S12a). Both spectra with PVK/SLGO and SLGO matrices exhibited $[M + Na]^+$ (m/z 188.19) and $[M + K]^+$ (Phe, m/z 204.19) peaks for phenylalanine, with PVK/SLGO exhibiting a higher signal-to-noise ratio than SLGO (Figure S12c and g). No phenylalanine peak was detected when PVK was used as the matrix because the matrix interference peak was dominant (Figure S12e). In the negative ion mode, the deprotonated $[M-H]^-$ ion (m/z 164.19) of phenylalanine was clearly detected using 9-AA and PVK matrices, and matrix-related peaks were observed at m/z 192.51 and 165, respectively (Figure S12b and f). The PVK/SLGO matrix yielded a clear and single deprotonated $[M-H]^-$ ion (m/z 164.19) for phenylalanine (Figure S12h), with a significantly higher signal-to-noise ratio (S/N) compared to that of the SLGO matrix (Figure S12d). To further verify that the PVK/SLGO composite matrix exhibits better matrix properties than the traditional CHCA and 9-AA matrices, proline, mannitol and palmitic acid were used as representative molecules for comparison (Figures S13 and S14).

https://doi.org/10.1021/acsomega.2c04772
ACS Omega 2022, 7, 39028−39038

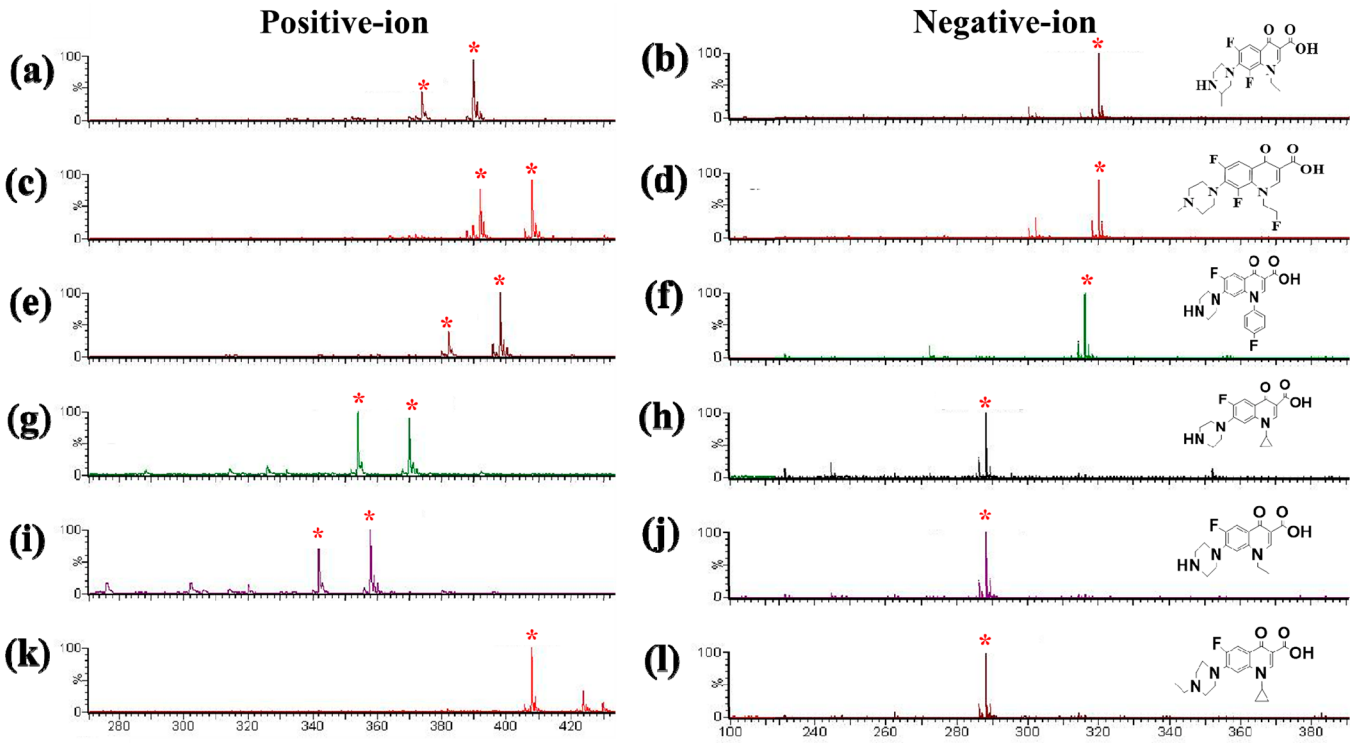

Figure 5. Mass spectra of (a, b) Lomefloxacin, (c, d) Fleroxacin, (e, f) Enrofloxacin, (g, h) Ciprofloxacin, (i, j) Norfloxacin, and (k, l) Sarfloxacin hydrochloride detected using PVK/SLGO as the MALDI matrix. The left and right columns show the spectra obtained in the positive and negative ion modes, respectively. The concentration of each analyte was 1 mg/mL.

Amino acids and nucleic acid bases play significant roles in various biological activities. The wide applicability of PVK/SLGO as a substrate was validated using various biologically relevant small molecules. Histidine, proline, and adenine were detected using the PVK@SLGO matrix in the positive ion mode (Figure 3, left), whereas proline, uracil, and thymine were detected in the negative ion mode (Figure 3, right). The characteristic peaks $[M + H]^+$, A, m/z 136.13; $[M + Na]^+$, His, m/z 178; Pro, m/z 138.13; A, m/z 158.22 and $[M + K]^+$, His, m/z 194; Pro, m/z 154.13; A, m/z 174.36 of the targets were observed in the positive ion mode (Figure 3a–c). The clear deprotonated peaks belonging to $[M-H]^-$ (marked with *), namely, Pro, m/z 114.13; T, m/z 125; and U, m/z 112 were observed in the negative ion mode (Figure 3d–f).

2.4. MALDI-TOF MS of Endocrine Disruptors in Environmental Samples. Bisphenol compounds (BPs) exert adverse effects on the human immune system as they act as endocrine disruptors.[49] To further verify the broad applicability of the PVK/SLGO matrix, bisphenol A, bisphenol B, bisphenol F, and bisphenol S (BPA, BPB, BPF, and BPS; m/z 228.29, 242.32, 200.24, and 250.27, respectively) were used as target analytes. In Figure 4a–d, the $[M-H]^-$ peak for BPA and its fragmentation $[M-CH_4-H]^-$ peak appeared at m/z 225.89 and 209.86, respectively. The peaks at m/z 239.90 and 209.87 belonging to BPB correspond to $[M-H]^-$ and $[M-C_2H_6-H]^-$, respectively. The peaks at m/z 199 and 197.90 belonging to BPF correspond to $[M-H]^-$ and its hydrogen rearrangement ion, respectively. The peak at m/z 248.58 for bisphenol S corresponds to the $[M-H]^-$ ion. Figure S15 shows a schematic of the fragmentation path of BPs in the negative ion mode.

2.5. MALDI-TOF MS of Quinolone Antibiotics. Misuse of quinolone antibiotics is harmful to humans; therefore, high analytical sensitivity and rapid screening are necessary. To test its applicability and further evaluate the PVK/SLGO matrix for small-molecule detection, six quinolone antibiotic drugs (lomefloxacin (LOM), fleroxacin (FLE), enrofloxacin (ENR), ciprofloxacin (CIP), norfloxacin(NOR), and safloxacin hydrochloride(SAR)) were selected for detection in the positive and negative ion modes (Figure 5). All six quinolone peaks were observed, and a good S/N was obtained. The PVK/SLGO matrix exhibited excellent signal intensities for the $[M + Na]^+$ and $[M + K]^+$ ions of all analytes except SAR, which only exhibited a $[M + Na]^+$ signal (Figure 5b). As presented in Figure 5b–l, the six quinolone peaks were observed using PVK/SLGO in the negative ion mode. The MS peaks were assigned to fragment ion $[M-C_2H_5]^-$ for LOM (m/z 320.19) and NOR (m/z 288.38; Figure 5b and j); $[M-C_2H_4F]^-$ for FLE (m/z 320.18; Figure 5d); $[M-C_3H_5]^-$ for ENR (m/z 316.25) and CIP (m/z 288.37; Figure 5f and h); and $[M-C_6H_4F]^-$ for SAR (m/z 288.37; Figure 5l). Figure S16 shows a schematic of the fragmentation path of quinolones in the negative ion mode.[50]

2.6. MALDI-TOF MS of Other Small Molecules. The small molecules, namely, mannitol (Ma, m/z 182.17), citric acid (CA, m/z 192.13), and palmitic acid (C16, m/z 256.42), were also examined. Figure 6a–c show the negative ion mass spectra of the three compounds with PVK/SLGO as a matrix. The single $[M-H]^-$ ions of the molecules were clearly detected (Figure 6a–c), confirming good matrix performance.

2.7. Salt Tolerance and Stability of the PVK/SLGO Matrix. Excessive salt in samples usually inhibits signal intensity in MALDI MS. Many biological samples contain high salt concentrations; therefore, the salt tolerance of the PVK/SLGO matrix was assessed using histidine (Figure 7a). The signal intensity of the $[M + Na]^+$ (m/z 178) ion peak of

https://doi.org/10.1021/acsomega.2c04772
ACS Omega 2022, 7, 39028−39038

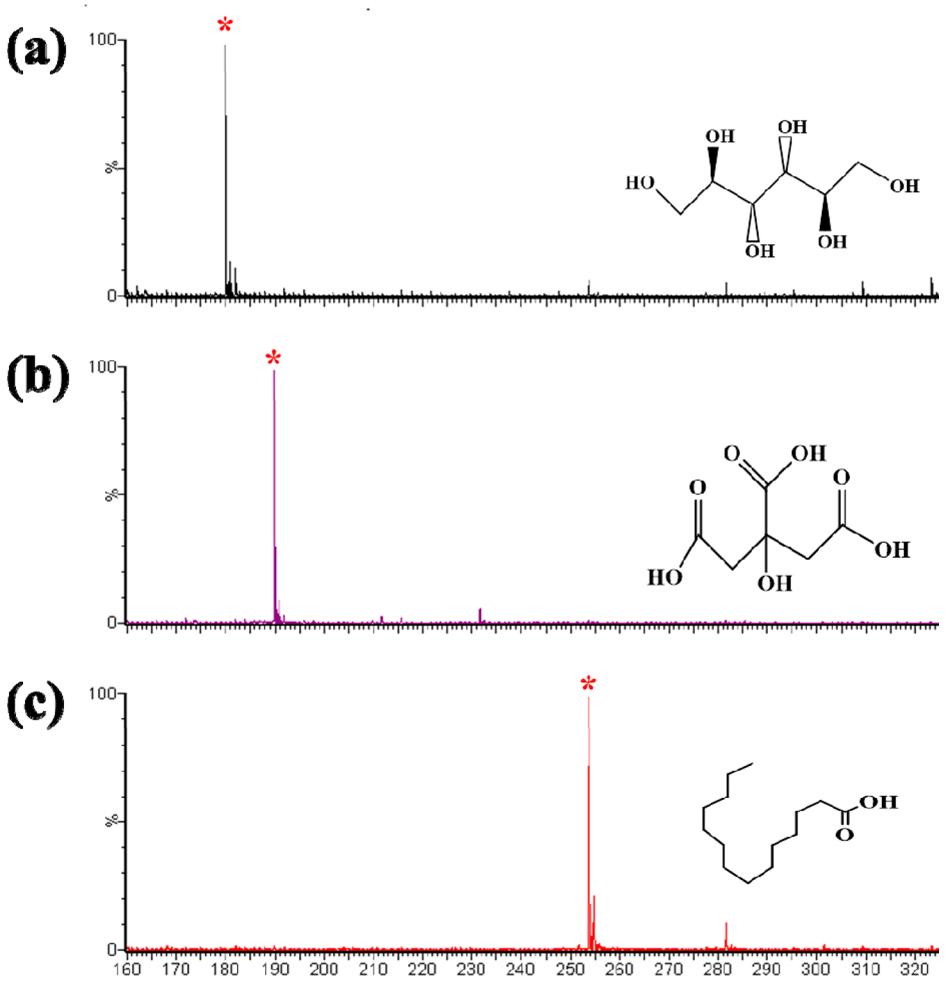

Figure 6. Negative-ion-mode MALDI mass spectra of (a) mannitol, (b) citric acid, and (c) palmitic acid using the PVK/SLGO matrix (analyte concentration: 1 mg/mL).

His showed slight differences with increasing NaCl concentration. The $[M + K]^+$ (m/z 194) ion peak of His was detected when 0 mmol/L NaCl was added, while the $[M + 2Na - H]^+$ (m/z 200) ion peak was detected at 10−1000 mmol/L NaCl, with oscillating signal intensity. These results indicate that the PVK/SLGO matrix exhibits high salt tolerance.

Good matrix stability allows for the exploration of analytical performance. Briefly, 2 mg/mL of the PVK/SLGO matrix was stored at 4 °C for 1, 7, 14, and 28 days and subsequently mixed with 1 mg/mL histidine. Then, 2 μL of the mixed solution was spotted on a target plate and dried at room temperature. Mass spectrometric detection was performed to study the stability of the PVK/SLGO matrix. PVK/SLGO exhibited very good stability for 28 consecutive days with insignificant signal intensity reduction of the target (Figure 7b), indicating that PVK/SLGO is an extremely stable matrix.

2.8. Determination of ENR in Milk Samples. A MALDI-TOF MS method for the quantitative analysis of ENR was established using a stable isotope internal standard (ENR-d5). Figure 8a shows that both ENR and ENR-d5 peaks were detected with $[M-C_3H_5]^-$ using the PVK/SLGO matrix in the negative ion mode. A good linear relationship was obtained between the ion intensity ratio of $[ENR-C_3H_5]^-$ and $[ENR-d5-C_3H_5]^-$ and the concentration ratio of ENR and ENR-d5 over a concentration range of 0.0001−0.1 (Figure 8a, inset). Measurement repeatability was investigated by quantifying the positive milk samples with a spiked concentration of 0.1 mg/mL ENR, and the results are listed in Table S2. The relative standard deviations within and between groups were <6%, with good precision. The recoveries of the milk samples spiked with 0.005, 0.01, and 0.1 mg/mL ENR were 102%, 113.6%, and 103.7%, respectively, with overall relative standard deviations of <15%, indicating that the newly established method for quantitative analysis of milk samples exhibited good measurement accuracy (Table S3). The limits of detection and quantification were calculated from the ENR concentration in the sample corresponding to 3 and 10 times the signal-to-noise ratio, respectively, and were determined to be 0.0001 and 0.005 mg/mL, respectively (Figure S17).

2.9. Mechanism of the Improved Ionization Efficiency Achieved by the PVK/SLGO Matrix. The effect of PVK/SLGO on the desorption efficiency was further investigated. As shown in Figure S18, the MALDI signal of histidine significantly improved with the composite PVK/SLGO matrix, indicating that the novel matrix promoted the desorption and ionization of the target. The mechanism of the improved ionization efficiency was further explored. Figure 8b presents the XPS profiles of PVK/SLGO, where a C 1s peak at 284.88 eV was identified as sp^2 bound carbon from C═C and C═O, verifying the presence of the successive π conjugation structure of SLGO. The C 1s peak at 286.98 eV was assigned to the weaker sp^3 carbon in C−O bonds, and the C 1s peak at 285.98

https://doi.org/10.1021/acsomega.2c04772
ACS Omega 2022, 7, 39028−39038

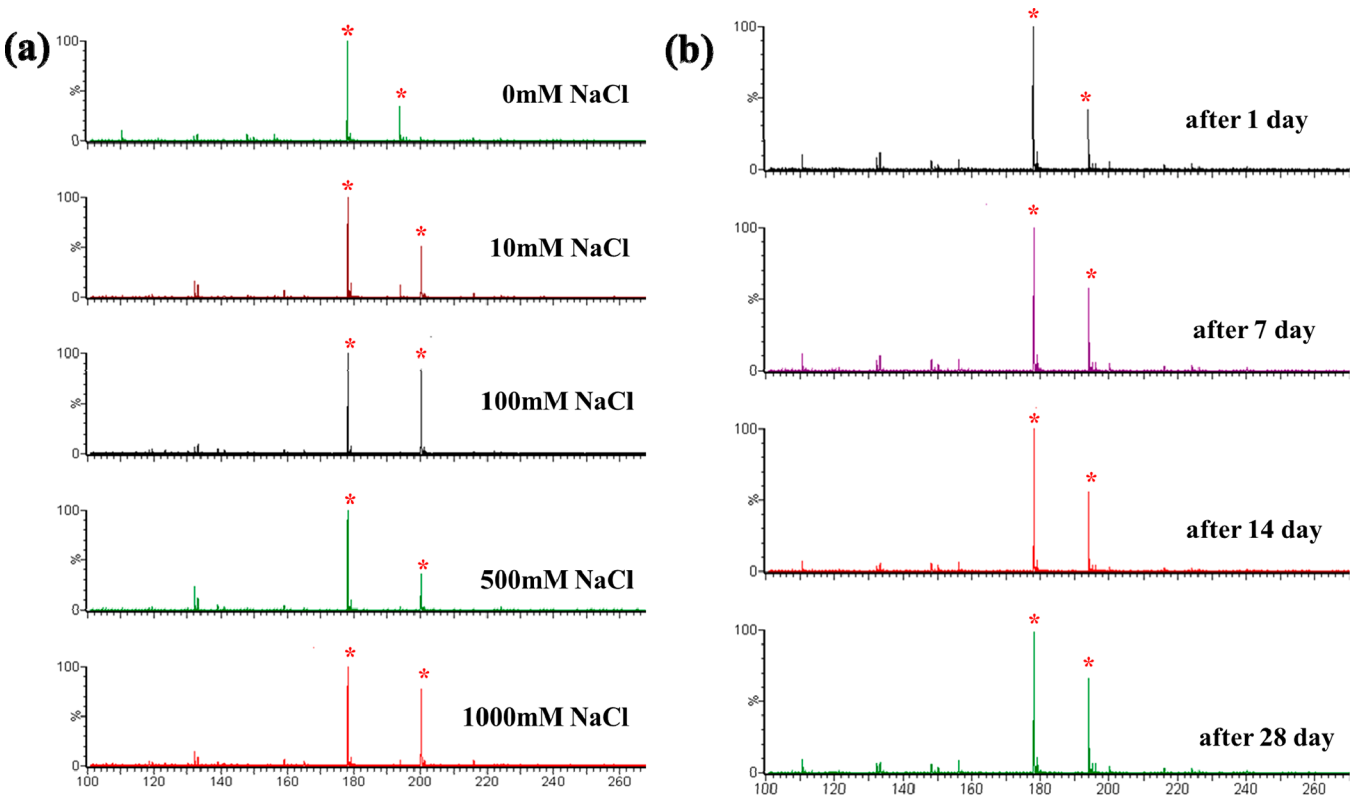

Figure 7. (a) MALDI-TOF MS spectra of His (1 mg/mL) using the PVK/SLGO matrix in 0−1000 mM NaCl. (b) MALDI-TOF MS spectra of His (1 mg/mL) using the PVK/SLGO matrix stored for 1, 7, 14, and 28 days.

eV was assigned to the C−N bonds of PVK. The O 1s peaks at 532.68 and 533.2 eV indicate that oxygen mainly exists in C═O and C−O on the surface of SLGO. The N 1s peak at 399.68 eV indicates that N mainly exists as C−N with the lone-pair electrons in PVK acting as Lewis bases with strong electron-donating effects. As a major component of SLGO, oxygen atoms in carboxyl and hydroxyl groups can act as Lewis acids and transfer protons to the analyte during desorption. This is conducive to PVK enhancing the ionization efficiency of the MALDI-TOF MS analyte in the positive ion mode. Hence, the PVK/SLGO composite can enable positive and negative dual-ion mode detection. In addition, the matrix must exhibit strong UV absorption within the laser emission wavelength (337 nm) to facilitate the ionization of the analyte molecules in the gas phase. As shown in Figure 1i, the composite PVK/SLGO solution showed stronger absorbance than the SLGO matrix at ∼250 nm, which is conducive to the improvement of absorption and energy transfer. This originates from the successive π conjugate structure and hydrogen bond interactions between PVK and SLGO. Finally, the SLGO matrix inhibited the ionization of PVK and improved the S/N of the obtained spectra. As shown in Figure S11d, the PVK matrix exhibited matrix-related peaks at m/z 165. However, after the addition of SLGO to the composite, the matrix background was greatly reduced, and no PVK-related peaks were observed (Figure S11b). These synergistic effects enhanced the performance of the PVK/SLGO matrix and facilitated small-molecule analysis by MALDI-TOF MS.

3. CONCLUSIONS

In this study, PVK/SLGO composites were prepared by combining the advantages of amorphous nitrogen heterocyclic homopolymer PVK and inorganic nanomaterial SLGO. Amino acids, nucleic acid bases, environmental endocrine disruptors, quinolone antibiotics, and other small molecules were detected by MALDI MS using the newly prepared PVK/SLGO matrix in the positive and negative dual-ion mode. The background peak interference in the low-molecular-weight region was eliminated, and the signal intensity of the analytes and detection sensitivity were thereby improved. Furthermore, the PVK/SLGO matrix exhibited high salt tolerance and stability, and its ionization mechanism involved the two materials acting synergistically. MALDI-TOF MS quantitation of ENR in milk samples was realized by introducing an isotopic internal standard, ENR-d5, in the negative ion mode. PVK/SLGO exhibited excellent efficiency as a dual-ion mode MALDI matrix with considerable potential for the imaging analysis of biological samples.

4. METHODS

Chemicals and Reagents. SLGO and PVK were purchased from Budweiser Chemical Reagent Co., Ltd. (Beijing, China). α-Cyano-4-hydroxycinnamic acid (CHCA), trifluoroacetic acid (TFA), methanol, phenylalanine (Phe), proline (Pro), histidine (His), lysine (Lys), adenine (A), uracil (U), thymine (T), lomefloxacin (LOM), fleroxacin (FLE), enrofloxacin (ENR), ciprofloxacin (CIP), norfloxacin (nor), safloxacin hydrochloride (SAR), bisphenol A (BPA), bisphenol B (BPB), bisphenol F (BPF), bisphenol S (BPS), tetraethylammonium chloride (TC), annitol (MA), citric acid (CA), and palmitic acid (C16) were purchased from Sigma-Aldrich (USA). Milk was purchased from a local shop. All chemicals were used as received without further purification. Ultrapure

https://doi.org/10.1021/acsomega.2c04772
ACS Omega 2022, 7, 39028−39038

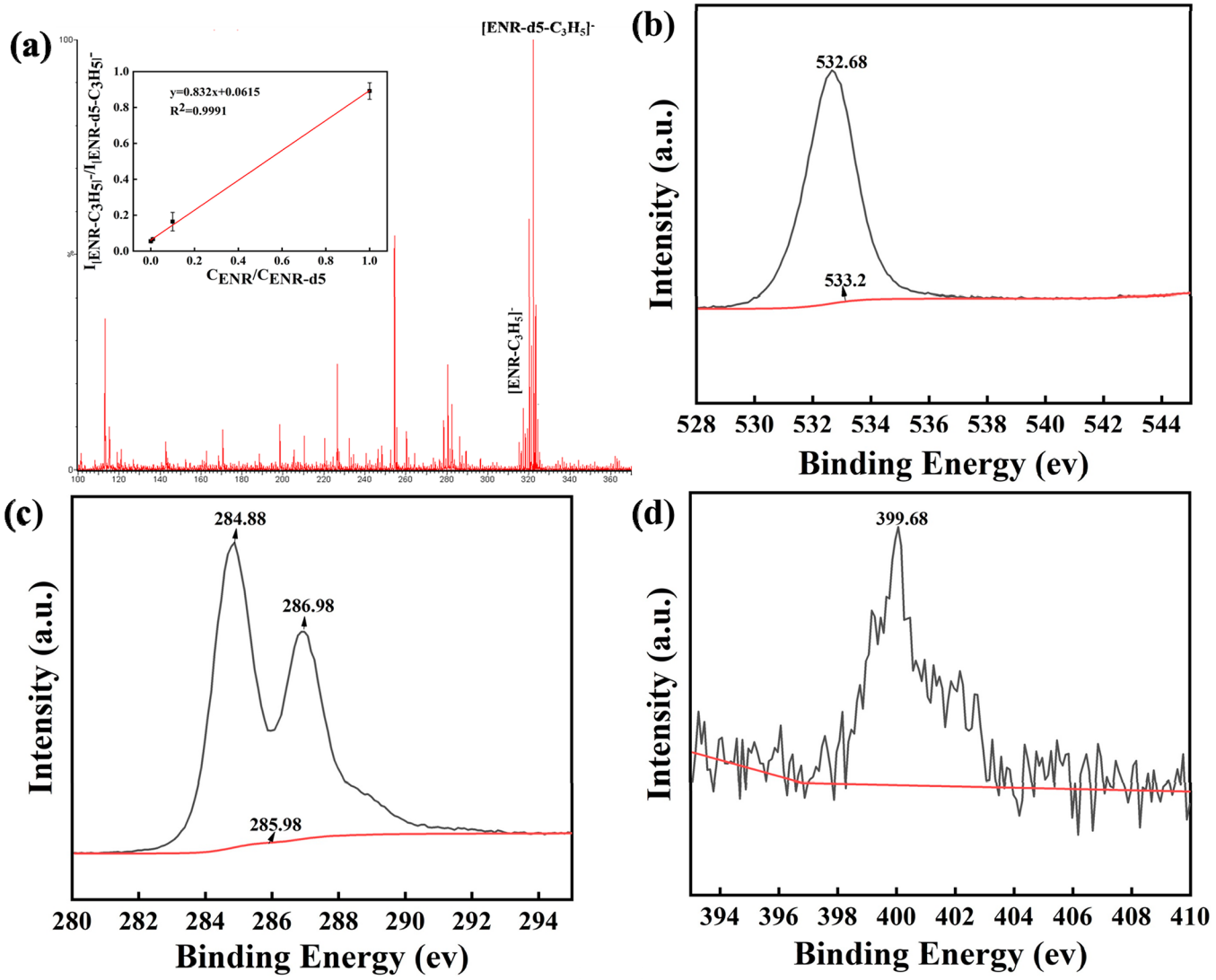

Figure 8. (a) MALDI-TOF MS of ENR in milk with a spiked concentration of 0.1 mg/mL using the PVK/SLGO matrix in the negative ion mode. Inset: linear relationship between the concentration ratio of ENR and ENR-d5 and the ion intensity ratio of $[ENR-C_3H_5]^-$ and $[ENR\text{-}d5-C_3H_5]^-$, (b) C 1s spectra, (c) O 1s spectra, and (d) N 1s spectra of PVK/SLGO.

water with an electrical resistance of >18.2 MΩ from Milli-Q was used for all experiments.

Apparatus. Scanning electron microscopy (SEM) images were obtained using a SUPRA 55VP instrument (Carl Zeiss, Germany). X-ray diffraction (XRD) patterns were recorded using a SmartLab 9 automated multipurpose X-ray diffractometer (Rigaku, Japan) with Cu Kα radiation (λ = 1.54056 Å). X-ray photoelectron spectroscopy (XPS) measurements were performed using an ESCALAB 250Xi X-ray photoelectron spectrometer (Thermo Fisher Scientific, USA). Fourier-transform infrared (FT-IR) spectra were recorded using a Nicolet 380 FT-IR spectrometer (Thermo Fisher Scientific, USA) with KBr as the background. Raman spectra were obtained using a Renishaw in Via confocal Raman microscope. Thermogravimetric analysis (TGA) was conducted with a TGA/DSC 1 instrument (Mettler Toledo, Switzerland). UV−vis spectra were obtained using a UV-2600 double beam UV spectrophotometer (Golden Island, Japan).

■ ASSOCIATED CONTENT

Supporting Information

The Supporting Information is available free of charge at https://pubs.acs.org/doi/10.1021/acsomega.2c04772.

Details about the chemicals used, instrumentation employed, experimental settings, results of MALDI MS experiments, as well as results of XRD, XPS, and Raman analyses (PDF)

■ AUTHOR INFORMATION

Corresponding Authors

Tie Han − *Tianjin Key Laboratory of Risk Assessment and Control Technology for Environment and Food Safety, Tianjin Institute of Environmental and Operational Medicine, Tianjin 300050, China*; Email: 524608150@qq.com

Huanying Zhou − *Tianjin Key Laboratory of Risk Assessment and Control Technology for Environment and Food Safety, Tianjin Institute of Environmental and Operational*

https://doi.org/10.1021/acsomega.2c04772
ACS Omega 2022, 7, 39028−39038

Medicine, Tianjin 300050, China; orcid.org/0000-0002-2453-3982; Email: zhouhytj@163.com

Authors

Xiuying Chen − *Key Laboratory of Medicinal Chemistry and Molecular Diagnosis, College of Chemical and Environmental Sciences, Hebei University, Baoding 071002, China; Tianjin Key Laboratory of Risk Assessment and Control Technology for Environment and Food Safety, Tianjin Institute of Environmental and Operational Medicine, Tianjin 300050, China; Nanpu Development Zone Administrative Examination and Approval Bureau, Tangshan 063305, China;* orcid.org/0000-0002-7039-5410

Yonghui Wang − *Tianjin Key Laboratory of Risk Assessment and Control Technology for Environment and Food Safety, Tianjin Institute of Environmental and Operational Medicine, Tianjin 300050, China*

Yuanyuan Luo − *Tianjin Key Laboratory of Risk Assessment and Control Technology for Environment and Food Safety, Tianjin Institute of Environmental and Operational Medicine, Tianjin 300050, China*

Zhixian Gao − *Tianjin Key Laboratory of Risk Assessment and Control Technology for Environment and Food Safety, Tianjin Institute of Environmental and Operational Medicine, Tianjin 300050, China;* orcid.org/0000-0003-2818-6671

Complete contact information is available at: https://pubs.acs.org/10.1021/acsomega.2c04772

Notes

The authors declare no competing financial interest.

■ ACKNOWLEDGMENTS

This work was supported by the National Key Research and development program of China [grant number: 2017YFF0211301].

■ ABBREVIATIONS

Matrix-assisted laser desorption ionization time-of-flight mass spectrometry, MALDI-TOF MS; single-layer graphene oxide, SLGO; poly n-vinylcarbazole, PVK; 9-aminoacridine, 9-AA; α-cyano-4-hydroxycinnamic acid, CHCA; enrofloxacin, ENR; carbon quantum dots, CDs; 3-hydroxypicolinic acid, HPA; phenylalanine, Phe; histidine, His; proline, Pro; adenine, A; uracil, U; thymine, T; bisphenol A, BPA; bisphenol B, BPB; bisphenol F, BPF; bisphenol S, BPS; lomefloxacin, LOM; fleroxacin, FLE; enrofloxacin, ENR; ciprofloxacin, CIP; norfloxacin, NOR; safloxacin hydrochloride, SAR; mannitol, Ma; citric acid, CA; palmitic, C16; signal-to-noise, S/N

■ REFERENCES

(1) Karas, M.; Hillenkamp, F. Laser desorption ionization of proteins with molecular masses exceeding 10,000 Da. *Anal. Chem.* **1988**, *60* (20), 2299−2301.

(2) Wu, J.; Ouyang, D.; He, Y. T.; Su, H.; Yang, B. C.; Li, J.; Sun, Q. Q.; Lin, Z. A.; Cai, Z. W. Synergistic Effect of Metal-Organic Framework/Gallic Acid in Enhanced Laser Desorption /Ionization Mass Spectrometry. *ACS Appl. Mater. Interfaces* **2019**, *11*, 38255−38264.

(3) Yang, J.; Wang, R.; Huang, L.; Zhang, M. J.; Niu, J. Y.; Bao, C. D.; Shen, N.; Dai, M.; Guo, Q.; Wang, Q.; et al. Urine Metabolic Fingerprints Encode Subtypes of Kidney Diseases. *Angew. Chem., Int. Ed.* **2020**, *59*, 1703−1710.

(4) Ouyang, D.; Zheng, Q.; Huang, H.; Cai, Z. W.; Lin, Z. A. Covalent Organic Framework Nanofilm-Based Laser Desorption/Ionization Mass Spectrometry for 5-Fluorouracil Analysis and Tissue Imaging. *Anal. Chem.* **2021**, *93* (47), 15573−15578.

(5) Wei, J.; Buriak, J. M.; Siuzdak, G. Desorption-ionization mass spectrometry on porous silicon. *Nature* **1999**, *399* (6733), 243−246.

(6) McLean, J. A.; Stumpo, K. A.; Russell, D. H. Size-selected (2−10 nm) gold nanoparticles for matrix assisted laser desorption ionization of peptides. *J. Am. Chem. Soc.* **2005**, *127* (15), 5304−5305.

(7) Lin, Z. A.; Zheng, J. N.; Bian, W.; Cai, Z. W. $CuFe_2O_4$ magnetic nanocrystal clusters as a matrix for the analysis of small molecules by negative-ion matrix-assisted laser desorption/ionization time-of-flight mass spectrometry. *Analyst* **2015**, *140*, 5287−5294.

(8) Shrivas, K.; Hayasaka, T.; Sugiura, Y.; Setou, M. Method for simultaneous imaging of endogenous low molecular weight metabolites in mouse brain using TiO_2 nanoparticles in nanoparticle-assisted laser desorption/ ionization-imaging mass spectrometry. *Anal. Chem.* **2011**, *83* (19), 7283−7289.

(9) Li, Z.; Zhang, Y. W.; Xin, Y. L.; Bai, Y.; Zhou, H. H.; Liu, H. W. A lithium rich composite metal oxide used as a SALDI-MS matrix for the determination of small biomolecules. *Chem. Commun.* **2014**, *50* (97), 15397−15399.

(10) Xu, S. Y.; Li, Y. F.; Zou, H. F.; Qiu, J. S.; Guo, Z.; Guo, B. C. Carbon nanotubes as assisted matrix for laser desorption/ionization time-of-flight mass spectrometry. *Anal. Chem.* **2003**, *75* (22), 6191−6195.

(11) Tang, H. W.; Ng, K. M.; Lu, W.; Che, C. M. Ion desorption efficiency and internal energy transfer in carbon-based surface-assisted laser desorption/ ionization mass spectrometry: desorption mechanism(s) and the design of SALDI substrates. *Anal. Chem.* **2009**, *81* (12), 4720−4729.

(12) Coffinier, Y.; Szunerits, S.; Drobecq, H.; Melnyk, O.; Boukherroub, R. Diamond nanowires for highly sensitive matrix-free mass spectrometry analysis of small molecules. *Nanoscale* **2012**, *4* (1), 231−238.

(13) Sunner, J.; Dratz, E.; Chen, Y. C. Graphite surface-assisted laser desorption/ionization time-of-flight mass spectrometry of peptides and proteins from liquid solutions. *Anal. Chem.* **1995**, *67* (23), 4335−4342.

(14) Meng, J. R.; Shi, C. Y.; Deng, C. H. Facile synthesis of water-soluble multi-wall carbon nanotubes and polyaniline composites and their application in detection of small metabolites by matrix assisted laser desorption/ ionization mass spectrometry. *Chem. Commun.* **2011**, *47* (39), 11017−11019.

(15) Dong, X.; Cheng, J.; Li, J.; Wang, Y. Graphene as a novel matrix for the analysis of small molecules by MALDI-TOF MS. *Anal. Chem.* **2010**, *82* (14), 6208−6214.

(16) Bolotin, K. I.; Sikes, K. J.; Jiang, Z.; Klima, M.; Fudenberg, G.; Hone, J.; Kim, P.; Stormer, H. L. Ultrahigh electron mobility in suspended grapheme. *Solid State Commun.* **2008**, *146* (9), 351−355.

(17) Kim, K. S.; Zhao, Y.; Jang, H.; Lee, S. Y.; Kim, J. M.; Kim, K. S.; Ahn, J. H.; Kim, P.; Choi, J. Y.; Hong, B. H. Large-scale pattern growth of graphene films for stretchable transparent electrodes. *Nature* **2009**, *457* (7230), 706−710.

(18) Chae, H. K.; Siberio-Pérez, D. Y.; Kim, J.; Go, Y.; Eddaoudi, M.; Matzger, A. J.; O'Keeffe, M.; Yaghi, O. M. A route to high surface area, porosity and inclusion of large molecules in crystals. *Nature* **2004**, *427* (6974), 523−527.

(19) Inagaki, M.; Kim, Y. A.; Endo, M. Graphene: preparation and structural perfection. *J. Mater. Chem.* **2011**, *21* (10), 3280−3294.

(20) Allen, M. J.; Tung, V. C.; Kaner, R. B. Honeycomb carbon: a review of graphene. *Chem. Rev.* **2010**, *110* (1), 132−45.

(21) Li, S. H.; Aphale, A. N.; Macwan, I. G.; Patra, P. K.; Gonzalez, W. G.; Miksovska, J.; Leblanc, R. M. Graphene Oxide as a Quencher for Fluorescent Assay of Amino acids, Peptides, and Proteins. *ACS Appl. Mater. Interfaces* **2012**, *4* (12), 7069−7075.

(22) Chuang, C.-H.; Wang, Y.-F.; Shao, Y.-C.; Yeh, Y.-C.; Wang, D.-Y.; Chen, C.-W.; Chiou, J. W.; Ray, S. C.; Pong, W. F.; Zhang, L.; Zhu, J. F.; Guo, J. H. The effect of thermal reduction on the

photoluminescence and electronic structures of graphene oxides. *Sci. Rep.* **2015**, *4* (1), 4525−4531.
(23) Cao, L.; Meziani, M. J.; Sahu, S.; Sun, R. P. Photoluminescence properties of graphene versus other carbon nanomaterials. *Accounts of chemical research* **2013**, *46* (1), 171−180.
(24) Tu, Y. Q.; Li, W.; Wu, P.; Zhang, H.; Cai, C. X. Fluorescence quenching of graphene oxide integrating with the site-specific cleavage of the endonuclease for sensitive and selective micro RNA detection. *Anal. Chem.* **2013**, *85* (4), 2536−2542.
(25) Shi, Y.; Dai, H. C.; Sun, Y. J.; Hu, J. T.; Ni, P. J.; Li, Z. Fluorescent sensing of cocaine based on a structure switching aptamer, gold nanoparticles and graphene oxide. *Analyst* **2013**, *138* (23), 7152−7156.
(26) Shang, J. Z.; Ma, L.; Li, J. W.; Ai, W.; Yu, T.; Gurzadyan, G. G. Femtosecond pump-probe spectroscopy of graphene oxide in water. *J. Phys. D: Appl. Phys.* **2014**, *47* (9), 094008−094014.
(27) Dikin, D. A.; Stankovich, S.; Zimney, E. J.; Piner, R. D.; Dommett, H. B.; Evmenenko, G.; Nguyen, S. T.; Ruoff, R. S. Preparation and characterization of graphene oxide paper. *Nature* **2007**, *448* (7152), 457−460.
(28) Jung, I.; Pelton, M.; Piner, R.; Dikin, D. A.; Stankovich, S.; Watcharotone, S.; Hausner, M.; Ruoff, R. S. Simple approach for high-contrast optical imaging and characterization of graphene-based sheets. *Nano Lett.* **2007**, *7* (12), 3569−3575.
(29) Paredes, J. I.; Villar-Rodil, S.; Martinez-Alonso, A.; Tascón, J. M. D. Graphene oxide dispersions in organic solvents. *Langmuir* **2008**, *24* (19), 10560−10564.
(30) Hamwi, A.; Marchand, V. Some chemical and electrochemical properties of graphite oxide. *J. Phys. Chem. Solids* **1996**, *57* (6−8), 867−872.
(31) Mermoux, M.; Chabre, Y.; Rousseau, A. FTIR AND ^{13}C NMR STUDY OF GRAPHITE OXIDE. *Carbon* **1991**, *29* (3), 469−474.
(32) Chen, X. Y.; Wang, Y. H.; Ren, S. Y.; Li, S.; Wang, Y.; Qin, K.; Li, S.; Han, D. P.; Peng, Y.; Han, T.; et al. Amorphous poly-N-vinylcarbazole polymer as a novel matrix for the determination of low molecular weight compounds by MALDI-TOF MS. *RSC Adv.* **2022**, *12*, 15215−15221.
(33) Zhao, H. F.; Li, Y. Q.; Wang, J.; Cheng, M.; Zhao, Z.; Zhang, H. N.; Wang, C. W.; Wang, J. Y.; Qiao, Y.; Wang, J. Z. Dual-Ion-Mode MALDI MS Detection of Small Molecules with the O-P, N-Doped Carbon/Graphene Matrix. *ACS Appl. Mater. Interfaces* **2018**, *10* (43), 37732−37742.
(34) Chen, S. M.; Zheng, H. Z.; Wang, J. N.; Hou, J.; He, Q.; Liu, H. H.; Xiong, C. Q.; Kong, X. L.; Nie, Z. X. Carbon Nanodots as a Matrix for the Analysis of Low-Molecular Weight Molecules in Both Positive-and Negative-Ion Matrix-Assisted Laser Desorption/Ionization Time-of-Flight Mass Spectrometry and Quantification of Glucose and Uric Acid in Real Samples. *Anal. Chem.* **2013**, *85* (14), 6646−6652.
(35) Yatim, A. R. M.; Wan Muhammad Zulkifli, W. N. F.; Majid, A. M. S.; Foster, J. L.; Hayes, D. G. 3-Hydroxypicolinic Acid as an Effective Matrix for Sophorolipid Structural Elucidation Using Matrix-Assisted Laser Desorption Ionization Time-of-Flight Mass Spectrometry. *Surfactants Deterg* **2020**, *23* (3), 565−571.
(36) Horatz, K.; Ditte, K.; Prenveille, T.; Zhang, K. N.; Jehnichen, D.; Kiriy, A.; Voit, B.; Lissel, F. Amorphous Conjugated Polymers as Efficient Dual-Mode MALDI Matrices for Low-Molecular-Weight Analytes. *ChemPlusChem.* **2019**, *84* (9), 1338−1345.
(37) Horatz, K.; Giampà, M.; Karpov, Y.; Sahre, K.; Bednarz, H.; Kiriy, A.; Voit, B.; Niehaus, K.; Hadjichristidis, N.; Michels, D. L.; et al. Conjugated Polymers as a New Class of Dual-Mode Matrices for MALDI Mass Spectrometry and Imaging. *J. Am. Chem. Soc.* **2018**, *140* (36), 11416−11423.
(38) Guo, Z.; He, L. A binary matrix for background suppression in MALDI-MS of small molecules. *Anal. Bioanal. Chem.* **2007**, *387*, 1939−1944.
(39) Zhou, L. H.; Kang, G. Y.; Kim, K. P. A binary matrix for improved detection of phosphopeptides in matrix-assisted laser desorption/ ionization mass spectrometry. *Rapid Commun. Mass Spectrom.* **2009**, *23*, 2264−2272.
(40) Shanta, S. R.; Zhou, L. H.; Park, Y. S.; Kim, Y. H.; Kim, Y. j.; Kim, K. P. Binary matrix for MALDI imaging mass spectrometry of phospholipids in both ion modes. *Anal. Chem.* **2011**, *83*, 1252−1259.
(41) Calvano, C. D.; Monopoli, A.; Ditaranto, N.; Palmisano, F. 1,8-bis (dimethylamino) naphthalene/9-aminoacridine: a new binary matrix for lipid fingerprinting of intact bacteria by matrix assisted laser desorption ionization mass spectrometry. *Anal. Chim. Acta* **2013**, *798*, 56−63.
(42) Chen, Y. L.; Gao, D.; Bai, H. R.; Liu, H. X.; Lin, S.; Jiang, Y. Y. Carbon Dots and 9AA as a Binary Matrix for the Detection of Small Molecules by Matrix-Assisted Laser Desorption/Ionization Mass Spectrometry. *American Society for Mass Spectrometry* **2016**, *27*, 1227−1235.
(43) Wang, J.; Huang, T. F.; Zhang, L.; Yu, Q. J.; Hou, L. A. Dopamine crosslinked graphene oxide Membrane for simultaneous removal of organic pollutants and trace heavy metals from aqueous solution. *Environmental Technology* **2018**, *39* (23), 3055−3065.
(44) Dikin, D. A.; Stankovich, S.; Zimney, E. J.; Piner, R. D.; Dommett, H. B.; Evmenenko, G.; Nguyen, S. T.; Ruoff, R. S. Preparation and characterization of graphene oxide paper. *Nature* **2007**, *448* (7152), 457−460.
(45) Si, Y. C.; Samulski, E. T. Synthesis of Water Soluble Graphene. *Nano Lett.* **2008**, *8* (6), 1679−1682.
(46) Hou, C.; Zhang, Q.; Zhu, M.; Li, Y.; Wang, H. One-step synthesis of magnetically-functionalized reduced graphite sheets and their use in hydrogels. *Carbon* **2011**, *49* (1), 47−53.
(47) Ferrari, A. C.; Meyer, J. C.; Scardaci, V.; Casiraghi, C.; Lazzeri, M.; Mauri, F.; Piscanec, S.; Jiang, D.; Novoselov, K. S.; Roth, S.; Geim, A. K. Raman spectrum of graphene and graphene layers. *Phys. Rev. Lett.* **2006**, *97*, 13831−13840.
(48) Amantonico, A.; Oh, J. Y.; Sobek, J.; Heinemann, M.; Zenobi, R. Mass Spectrometric Method for Analyzing Metabolites in Yeast with Single Cell Sensitivity. *Angew. Chem., Int. Ed.* **2008**, *47*, 5382−5385.
(49) Wang, J. N.; Sun, J.; Wang, J. Y.; Liu, H. H.; Xue, J. J.; Nie, Z. X. Hexagonal boron nitride nanosheets as a multifunctional background-free matrix to detect small molecules and complicated samples by MALDI mass spectrometry. *Chem. Commun.* **2017**, *53* (58), 8114−8117.
(50) Ma, Y. R.; Zhang, X. L.; Zeng, T.; Cao, D.; Zhou, Z.; Li, W. H.; Niu, H. Y.; Cai, Y. Q. Polydopamine-Coated Magnetic Nanoparticles for Enrichment and Direct Detection of Small Molecule Pollutants Coupled with MALDI-TOF-MS. *ACS Appl. Mater. Interfaces* **2013**, *5* (3), 1024−1030.

https://doi.org/10.1021/acsomega.2c04772
ACS Omega 2022, 7, 39028−39038